NASA TM X-67846

NASA TECHNICAL MEMORANDUM

NASA TM X-67846

PERFORMANCE OF A BRAYTON-CYCLE POWER CONVERSION SYSTEM USING A HELIUM-XENON GAS MIXTURE

by Alfred S. Valerino and Lloyd W. Ream
Lewis Research Center
Cleveland, Ohio

TECHNICAL PAPER proposed for presentation at
1971 Intersociety Energy Conversion Engineering Conference
sponsored by the Society of Automotive Engineers
Boston, Massachusetts, August 3-6, 1971

ABSTRACT

A Brayton power conversion system was operated in an ambient environment with a gas mixture of helium and xenon. The system was operated at a compressor inlet temperature of 80° F through a compressor discharge pressure range from 20 to 45 psia and through a turbine inlet temperature range from 1300° to 1600° F. Results of system and component performances through the operating range of parameters are discussed.

Results of the investigation indicated a net engine efficiency (excluding heat losses from the heat source) of approximately 30 percent at a compressor discharge pressure of 45 psia and a turbine inlet temperature of 1600° F. The gross power output measured at the alternator terminals for this condition was 13.2 kW. Good agreement was obtained in a comparison of the compressor adiabatic efficiency with that obtained with the compressor tested with argon gas; compressor efficiencies of the order of 79 percent were obtained. With the blend of helium and xenon and with high turbine inlet temperatures (1300° to 1600° F) turbine static efficiency was slightly lower than with cold argon; the values were 87.5 percent and 88.8 percent with hot helium-xenon and cold argon, respectively. The heat-transfer effectiveness of 0.95 of the gas-to-gas recuperator agreed with the predicted value at a system pressure level of 45 psia. The head rise of the liquid coolant pump, approximately 193 ft at a design capacity of 3.7 gal/min, was considerably higher than the specified minimum value of approximately 159 ft.

E-6339

CONSIDERABLE EFFORT HAS BEEN expended by the NASA, Lewis Research Center, to demonstrate the capabilities of a long-life, space-oriented, multi-kilowatt Brayton cycle power system. The Brayton engine was designed to produce 2 to 10 kW of electrical power with a gas mixture of helium-xenon (molecular weight of 83.8) as the working fluid. The power conversion system of the engine employs a rotating unit (BRU) close-coupled to a heat exchanger unit (BHXU). The rotating unit consists of a turbine, an alternator and a compressor on a single shaft which is supported and retained by journal and thrust bearings operating on a film of the systems working fluid. Design rotative speed is 36,000 rpm. The heat exchanger unit consists of a gas-to-gas recuperator, a gas-to-liquid waste heat exchanger, and associated ducting. Much data on the behavior of the components and of the power conversion system operating with either air, argon, or krypton has been published (1 to 13)*. Few experimental data, however, have been obtained or published on the components and system performance with the helium-xenon gas mixture as the working fluid. The experimental performance of a power conversion system operating in a vacuum environment with helium-xenon is reported in Ref. 14.

This paper presents data obtained with a power conversion system operating in an ambient environment with the helium-xenon gas mixture as the working fluid. Tests' variables include a turbine inlet temperature range of 1300° to 1600° F, a compressor discharge pressure range of 20 to 45 psia at a compressor inlet temperature of 80° F. Performance of the turbine, the compressor, the recuperator, the waste heat exchanger, the engine liquid coolant pump, as well as the power conversion system, are presented.

GENERAL DESCRIPTION

A schematic diagram of the Brayton power conversion system is presented in Fig. 1. An electric heat source was installed between the BHXU high-pressure side outlet and the turbine inlet to provide the thermal energy for the system. Gas flows from the compressor discharge, through the gas-to-gas recuperator into the heat source. The heated gas passes through the turbine, into the BHXU low-pressure side where it gives up some of its heat content to the gas

*Numbers in parentheses designate References at end of paper.

entering the recuperator from the compressor. Gas then flows into the waste heat exchanger where sufficient heat is released to the liquid coolant to maintain a compressor inlet temperature of 80° F.

The Dow Corning liquid coolant is circulated by the coolant pump through the waste heat exchanger via a single path and through the alternator via either one and/or two paths. Heat added to the coolant is removed by means of a refrigeration unit.

Photographs of the BRU, BHXU and the electric heat source installed in the power conversion facility are presented in Figs. 2 and 3. The heat source-BHXU installation in the system support frame is shown in Fig. 2. The heat source and its inlet and outlet piping are covered with a micro-quartz blanket type insulation. The installation of the vertically-mounted BRU, with the turbine end up, and the BHXU is shown in Fig. 3.

High gas temperatures were measured with chromel-alumel type thermocouples; low gas temperatures and liquid temperatures were measured with iron constantin thermocouples. Strain-gage type transducers were employed to measure all of the absolute and differential pressures required for pressure measurements and for gas flow rate computations. Liquid flow rates were sensed by a turbine-type flow meter.

Rotative speed of the BRU shaft was obtained by means of a capacitance probe located near the BRU compressor journal bearings and by means of the alternator frequency. A speed controller described in Ref. 13 was utilized to operate in a safe-speed band.

The electrical power output of the alternator's three phases were each measured with root-mean square instruments.

PROCEDURE

During the test, constant values of turbine inlet and compressor inlet temperatures were maintained while the compressor discharge pressure was varied. Turbine inlet temperature was controlled by a closed-loop controller regulating the electrical power to the heat source. The compressor inlet temperature was maintained at 80° F by controlling the liquid coolant flow rate to the waste heat exchanger. Temperature of the coolant entering the waste heat exchanger was fixed at approximately 68° F. The compressor discharge pressure was varied by varying the gas system inventory.

The speed controller was not properly tuned during this test. The resultant rotative speed and, therefore, the alternator frequency were approximately 101 to 104 percent above the design values. Design rotative speed was 36,000 rpm; design alternator frequency was 1200 Hz.

DISCUSSION

COMPRESSOR - The radial-outflow compressor was designed for a nominal 6-kW net output (1). A photograph of the compressor vaned diffuser-scroll assembly and the impeller is shown in Fig. 4.

The characteristics of the BRU compressor are shown in Figs. 5, 6, and 7. The effects of compressor discharge static pressure on the static pressure ratio across the compressor and the adiabatic efficiency are presented in Fig. 5. At a constant turbine inlet temperature, the compressor discharge pressure has no significant effect on neither the static pressure ratio nor the efficiency; however, increasing the turbine inlet temperature resulted in slight increases in static pressure ratio. The static pressure ratio increased from approximately 1.91 to 1.94 when the turbine inlet temperature was increased from 1300° to 1600° F. The pressure ratio obtained at 1600° F is slightly higher than the value obtained with argon as reported in Ref. 8.

The adiabatic efficiency (Fig. 5(b)) is essentially independent of the turbine inlet temperature. The experimental efficiency of approximately 79 percent is in good agreement with the 79.5 percent obtained from the argon test of Ref. 8.

The efficiencies and the static pressure ratios of the compressor are presented in Fig. 6 in the conventional compressor format-viz., pressure ratio and efficiency versus equivalent flow rate.

The effect of the equivalent weight flow on the temperature rise ratio is presented in Fig. 7. There is relatively good agreement between the experimental data with helium-xenon and the argon data of Ref. 8-approximately 0.38 compared to 0.37 with argon.

TURBINE - Photographs of the rotor housing and the scroll assembly are presented in Figs. 8 and 9, respectively. The radial-inflow turbine was also designed for a nominal 6-kW system electric power (2).

The operating characteristics of the turbine are presented in Figs. 10, 11 and 12. Effects of the compressor discharge static pressure on

the turbine inlet to discharge static pressure ratio and on the turbine efficiency are shown in Fig. 10. Compressor discharge pressure shows no significant effect on the static pressure ratio (Fig. 10(a)). A slight increase in pressure ratio resulted with increasing turbine inlet temperature. Pressure ratios of approximately 1.77 and approximately 1.79 were obtained at turbine inlet temperatures of 1300° and 1600° F, respectively.

Increasing compressor discharge static pressure from 25 to 45 psia resulted in a slight increase of approximately 2 percentage points in turbine efficiency (Fig. 10(b)). The data indicates a slightly lower efficiency (87.5 percent at a compressor discharge pressure of 25 psia) when compared to the cold argon tests of Ref. 7 (88.8 percent). The turbine efficiency and the equivalent inlet-to-discharge static pressure ratios are plotted in the conventional manner against blade-to-jet speed ratio and equivalent weight flow in Figs. 11 and 12, respectively. Scatter exists in the data but, in general, the data is in close agreement with the argon data of Ref. 7.

HEAT EXCHANGER UNIT (BHXU) - The BHXU, shown in Fig. 13, consists of a gas-to-gas recuperator, a gas-to-liquid waste heat exchanger and the interconnecting ducting. The recuperator is a counterflow plate-fin unit with cross-flow, tri-angular end sections. The waste heat exchanger is a cross-counterflow, plate-fin unit. Manifolds are provided for the two units and are shaped to provide uniform flow. Ducts are attached to the manifolds for connections to the heat source and the rotating unit. A more detailed description of the BHXU and some performance data are presented in Ref. 3.

The performance characteristics of the BHXU has been determined for the operating conditions of the power conversion system. The performance is expressed in terms of the heat transfer effectiveness-i.e., the ratio of the temperature drop to the difference between the inlet temperature through each heat exchanger passage. To demonstrate the behavior of the BHXU in relation to the system operating conditions, the performance is presented as a function of the system pressure level at the compressor discharge.

The variation of recuperator heat transfer effectiveness with compressor discharge pressure at turbine inlet temperatures of 1600° and 1300° F is shown in Fig. 14. The effectiveness is relatively constant at a turbine inlet temperature of 1600° F through the compressor discharge pressure range. The experimental effectiveness of 0.95 obtained at a turbine inlet temperature of 1600° F at a compressor discharge pressure of 42.5 psia is in agreement with the predicted value. The effectiveness decreased slightly with increasing compressor discharge pressure when the turbine inlet temperature was reduced to 1300° F.

The change in heat transfer effectiveness of the waste heat exchanger obtained at a turbine inlet temperature of 1600° F with compressor discharge pressure is shown in Fig. 15. A small decrease, from approximately 0.97 to 0.95, resulted when the compressor discharge pressure was increased from 25 to 45 psia. The small drop in effectiveness occurs because of the combined increase of both the heat load and the heat transfer coefficient.

The variation of overall pressure drop ratio across the BHXU with compressor discharge pressure at a turbine inlet temperature of 1600° F is presented in Fig. 16. Increasing compressor discharge pressure from 20 to 45 psia resulted in a decrease in the overall pressure drop ratio from approximately 0.056 to 0.038.

LIQUID COOLANT PUMP - The motor driven pump, shown in Fig. 17, is an integral, hermetically-sealed unit consisting of a centrifugal pump and a three-phase 400-Hz motor mounted in a common housing. A complete description of the coolant pump unit is presented in Ref. 4. Input power to the pump unit was supplied by a three-phase, 400-Hz motor-generation set. The nominal speed of the pump unit is 11,000 rpm.

The head rise characteristic of the coolant pump is shown in Fig. 18. The operating characteristics indicate that the pump head rise is well over the specified minimum requirement of 159 ft at a flowrate of 3.7 gal/min. Experimental value of approximately 192 ft was obtained at the design flow condition.

ENGINE - The effects of compressor discharge pressure and turbine inlet temperature on the power output measured at the alternator terminals (gross power output) are presented in Fig. 19. Increasing compressor discharge pressure and the turbine inlet temperature resulted in increases in the gross power output. At turbine inlet temperatures of 1600° and 1400° F, at a compressor discharge pressure of 45 psia, the gross electrical power outputs were approximately 13.2 and 10 kW, respectively. At a compressor discharge pressure of 20 psia, the gross power outputs were approximately 4.5 and 3.3 kW, respectively.

The efficiencies of the engine are presented in Fig. 20. Since the electric heat source does not provide a good engine-heat-source simulation, the efficiency of the electric heat source is not taken into account in the computation of the engine efficiency. The thermal input to the engine is defined as the rate of enthalpy addition across the heater-that is, $wc_p\Delta T$, where w is flow rate, c_p is specific heat at constant pressure and ΔT is temperature rise from recuperator outlet to turbine inlet.

The engine gross efficiencies, based on the gross power outputs, are presented as a function of the system pressure level at various turbine inlet temperatures in Fig. 20(a). At a compressor discharge pressure of 45 psia the gross efficiency decreased from approximately 33.5 percent to approximately 28.5 percent when the turbine inlet temperature was decreased from 1600° to 1400° F. At all turbine inlet temperatures, decreasing the compressor discharge pressure resulted in decreases in gross efficiency.

Since the operation of the Brayton engine is self-sustaining, a housekeeping power requirement for engine auxiliaries must be considered. This auxiliary power requirement is 1.4 kW (5). The net power or the useful engine power therefore is the gross power output minus 1.4 kW.

The effects of compressor discharge pressure and turbine inlet temperature on the engine net efficiency is shown in Fig. 20(b). The net efficiency is defined in the Appendix. At 1600° and 1400° F turbine inlet temperatures at a compressor discharge static pressure of 45 psia, the net efficiencies obtained were approximately 30 and 25 percent, respectively. At a compressor discharge pressure of 20 psia, the net efficiencies were approximately 19 and 13 percent, respectively.

CONCLUDING REMARKS

The performance characteristics of a Brayton cycle power conversion system and of its components were obtained with a gas mixture of helium-xenon as the working fluid. Tests were conducted in an ambient environment through a compressor discharge pressure range, a turbine inlet temperature range, and at a constant compressor inlet temperature of 80° F. Results of the investigation indicate:

1. At a turbine inlet temperature of 1600° F and a compressor discharge pressure of 45 psia, a system net efficiency of approximately 30 percent resulted. The system efficiency does not include the electric heat source efficiency since it does not adequately simulate the engine heat source.

2. The compressor adiabatic efficiency, approximately 79 percent, is in good agreement with the 79.5 percent value obtained from the component test with argon gas.

3. The turbine efficiency of 87.5 percent was approximately one percentage point lower than the value obtained when the turbine was tested with cold argon gas.

4. The effectiveness of the recuperator portion of the heat exchanger unit was approximately 95 percent. This value agrees with the predicted effectiveness.

5. The head rise of approximately 193 ft obtained with the liquid coolant pump far exceeded the specified minimum requirement of 159 ft at a capacity of 3.7 gal/min.

APPENDIX

AP_G	alternator gross output power, kW
C_p	specific heat at constant pressure, ft-lb/(lb-°R)
E_R	recuperator heat transfer effectiveness, $(T_{R1}-T_{R2})/(T_{R1}-T_{R3})$
Ew	waste heat exchanger effectiveness (gas side), $(T_{R2}-T_{w1})/(T_{R2}-T_{w2})$
g	gravitational constant, 32.174 ft/sec^2
Δh_i	ideal specific work, Btu/lb
J	mechanical equivalent of heat, 778.16 ft-lb/Btu
P	static pressure, psia
T	total temperature, °F
U_t	blade tip velocity, ft/sec
V	absolute gas velocity, ft/sec
V_j	ideal jet speed corresponding to static pressure ratio across the turbine, $2gJ(\Delta h_i)$, ft/sec
w	flow rate, lb/sec
γ	ratio of specific heats, 1.667 for helium-xenon mixture
δ	ratio of inlet static pressure to U.S. standard sea-level pressure P/P^*
ϵ	function of γ used in relating parameters to those using air inlet conditions at U.S. standard sea-level conditions, $\left(\frac{0.740}{\gamma}\right)\left(\frac{\gamma+1}{2}\right)^{\gamma/\gamma-1}$

η_c compressor adiabatic temperature rise efficiency,

η_T turbine efficiency

η_G engine system gross efficiency, $AP_G/1.054\ WC_p(T_{TI}-T_{R4})$

η_N engine system net efficiency, $(AP_G-1.4)/1.054\ WC_p(T_{TI}-T_{R4})$

θ_c ratio of compressor inlet total temperature to U.S. standard sea-level temperature, T_{CI}/T^*

θ_{CR} squared ratio of critical velocity at the turbine inlet to critical velocity at U.S. standard sea-level temperature, $(V_{CR}/V^*_{CR})^2$

ν blade-jet speed ratio, U_t/V_j

Superscripts

* U.S. standard sea-level conditions (temperature equal to 518.7° R; pressure equal to 14.7 psia).

Subscripts

C_D compressor discharge

C_I compressor inlet

CR condition corresponding to Mach number of unity

EQ equivalent

TD turbine discharge

TI turbine inlet

R1 recuperator inlet low pressure side

R2 recuperator outlet low pressure side

R3 recuperator inlet high pressure side

R4 recuperator outlet high pressure side

W1 gas outlet side of waste heat exchanger

W2 liquid inlet side of waste heat exchanger

REFERENCES

1. Anon., "Design and Fabrication of the Brayton Cycle High Performance Compressor Research Package." AiResearch Mfg. Co. Rep. APS-5269-R, NASA CR-72533, November 29, 1967.

2. Anon., "Design and Fabrication of the Brayton Cycle High Performance Turbine Research Package." Report APS-5281-R, AiResearch Mfg. Co. Rep. APS-5281-R, NASA CR-72478, February 14, 1968.

3. G. N. Kaykaty, "Design Description and Performance Test Results from Two Identical Brayton Heat Exchanger Units." NASA TM X-52844, 1970.

4. A., C. Spagnuolo, R. R. Secunde, and J. R. Vrancik, "Performance of a Hermetic Induction Motor-Driven Pump for Brayton Cycle Heat Rejection Loop." NASA TM X-52698, 1969.

5. D. B. Fenn, J. N. Deyo, T. J. Miller, and R. W. Vernon, "Experimental Performance of a 2-15 Kilowatt Brayton Power System in the Space Power Facility Using Krypton." NASA TM X-52750, 1970.

6. A. S. Valerino, R. P. Macosko, A. S. Asadourian, T. P. Hecker, and R. Kruchowy, "Preliminary Performance of a Brayton-Cycle-Power-System Gas Loop Operating with Krypton over a Turbine Inlet Temperature Range of 1200° F to 1600° F." NASA TM X-52769, 1970.

7. W. J. Nusbaum and M. G. Kofskey, "Cold Performance Evaluation of 4.97-Inch Radial-Inflow Turbine Designed for Single-Shaft Brayton Cycle Space-Power System." NASA TN D-5090, 1969.

8. C. Weigel, Jr., E. R. Tysi, and C. L. Ball, "Overall Performance in Argon of 4.25-Inch Sweptback-Bladed Centrifugal Compressor." NASA TM X-2129, 1970.

9. D. G. Beremand, D. Namkoong, and R. Y. Wong, "Experimental Performance Characteristics of Three Identical Brayton Rotating Units." NASA TM X-52826, 1970.

10. R. Y. Wong, H. A. Klassen, R. C. Evans, and C. H. Winzig, "Preliminary Investigation of a Single-Shaft Brayton Rotating Unit Designed for a 2-to-10 Kilowatt Space Power Generation System." NASA TM X-1869, 1969.

11. D. S. Repas and R. A. Edkin, "Performance Characteristics of a 14.3-Kilowatt-Ampere Modified Lundell Alternator for 1200 Hertz Brayton-Cycle Space-Power System." NASA TN D-5405, 1969.

12. J. L. Klann, "Steady-State Analysis of a Brayton Space-Power System." NASA TN D-5673, 1970.

13. B. D. Ingle, H. L. Wimmer, and R. C. Bainbridge, "Steady-State Characteristics of a Voltage Regulator and a Parasitic Speed Controller on a 14.3-Kilovolt-Ampere, 1200-Hertz Modified Lundell Alternator." NASA TN D-5924, 1970.

14. R. W. Vernon and T. J. Miller, "Experimental Performance of a 2-15 Kilowatt Brayton Power System Using a Mixture of Helium and Xenon." NASA TM X-52936, 1970.

E-6339

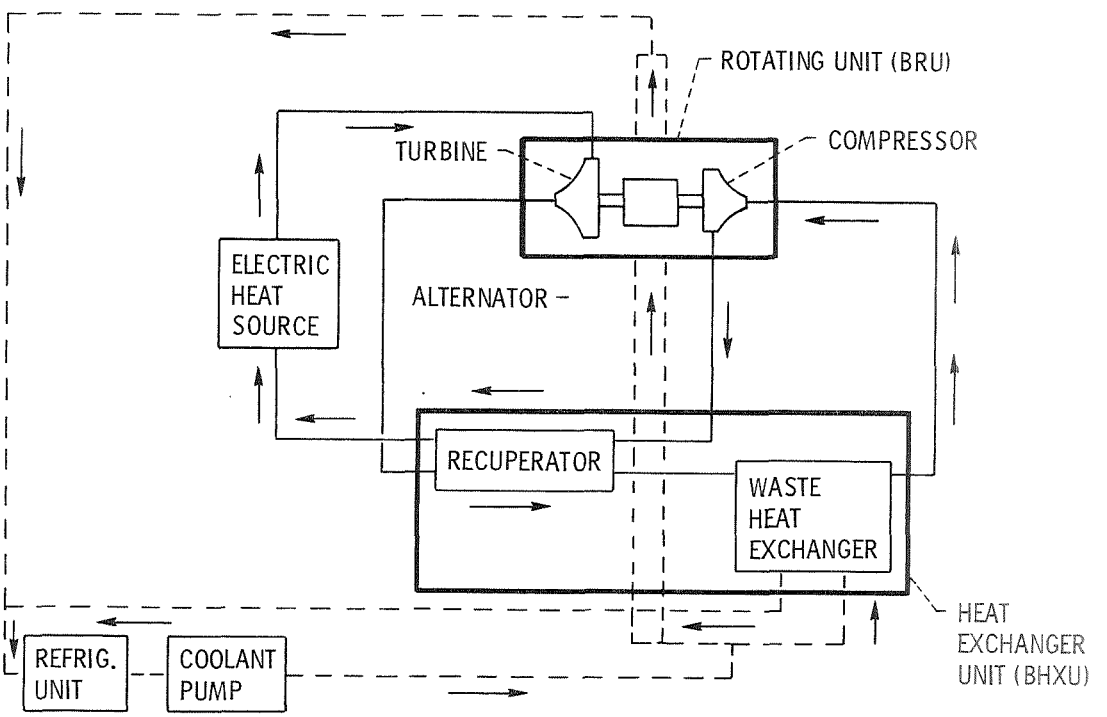

Figure 1. - Schematic of power conversion system.

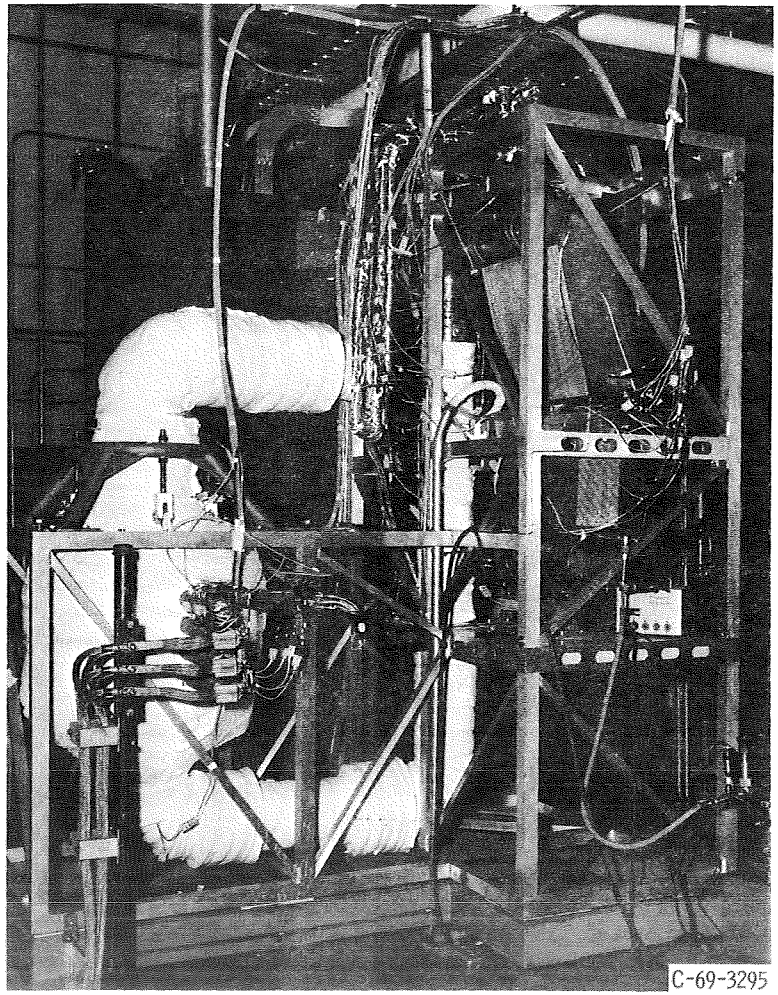

Figure 2. - Heat source - BHXU installation.

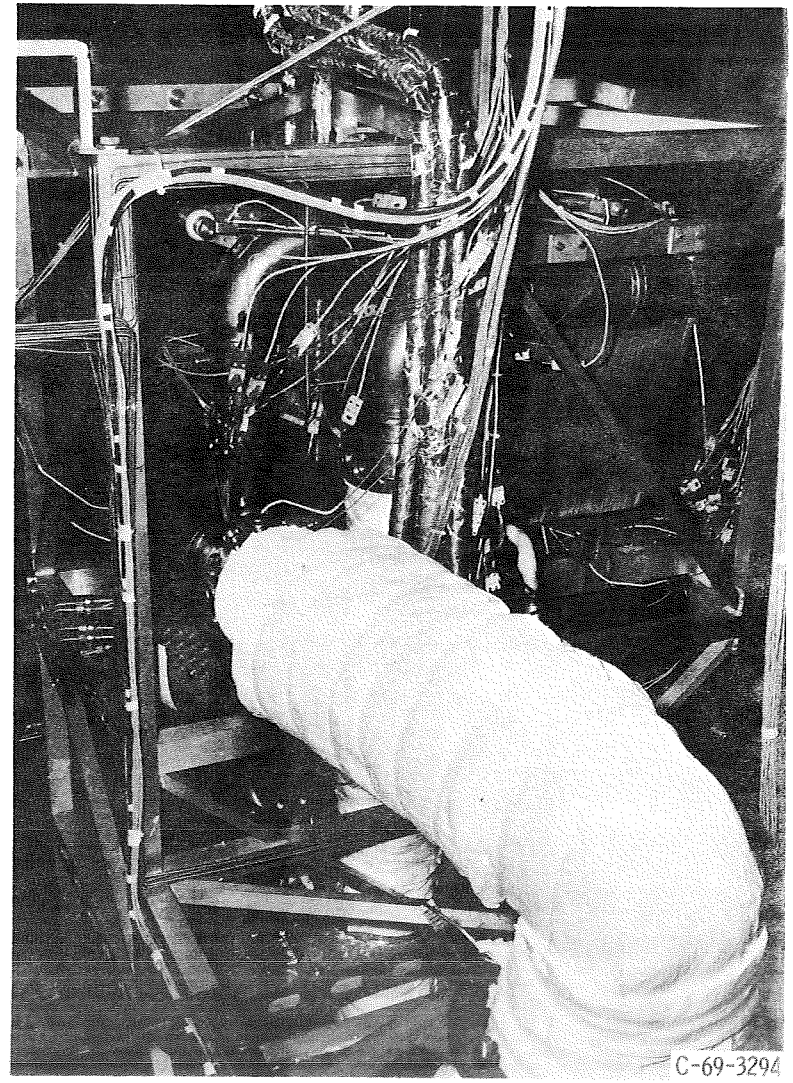

Figure 3. - Rotating unit - heat exchanger unit installation.

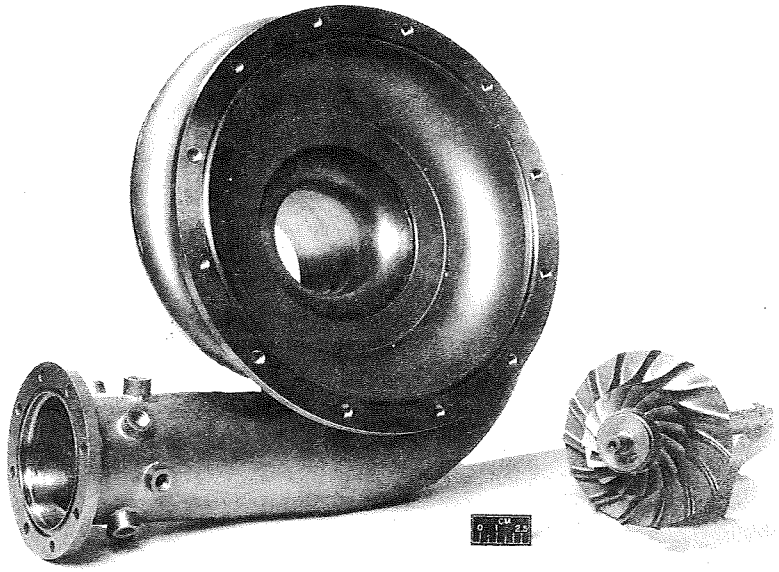

C-69-3758

Figure 4. - Compressor scroll and impeller.

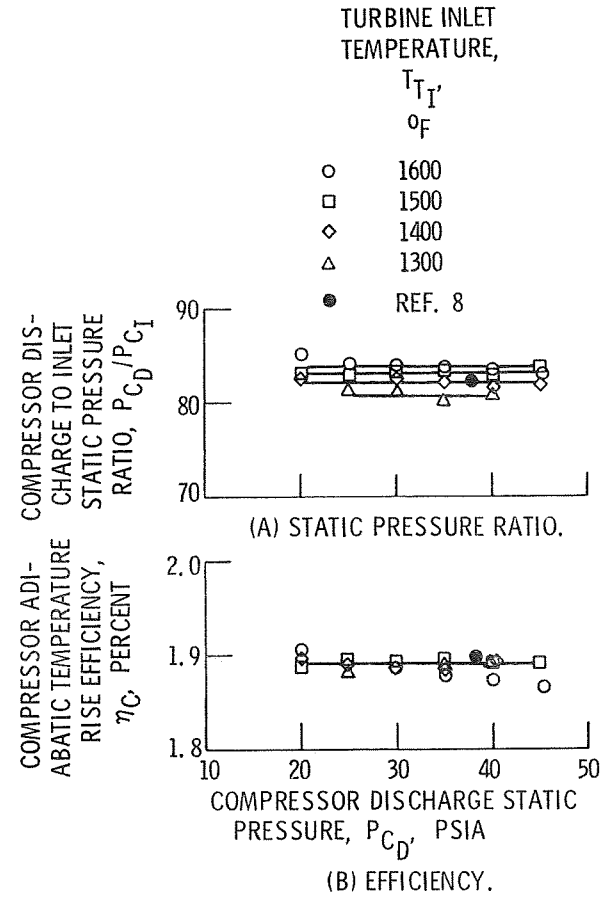

Figure 5. - Effect of compressor discharge pressure on compressor static pressure ratio and on compressor efficiency.

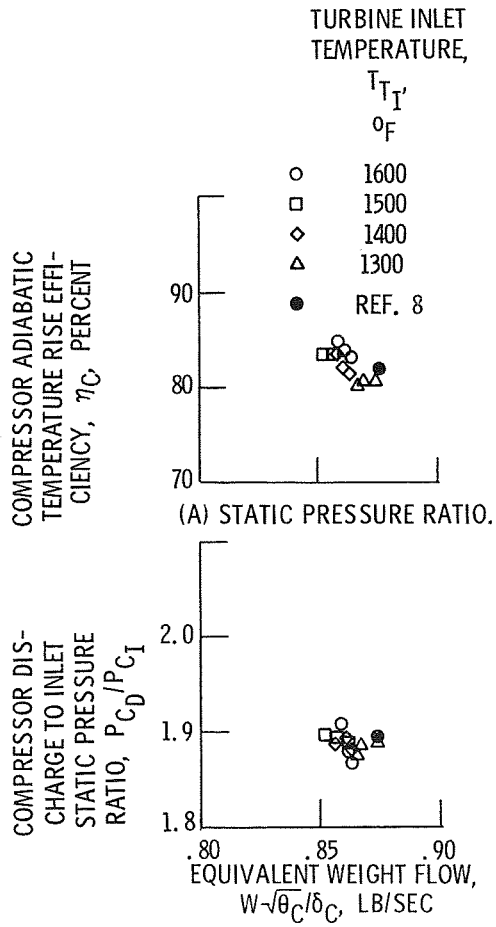

Figure 6. - Variation of compressor static pressure ratio and efficiency with equivalent flow rate.

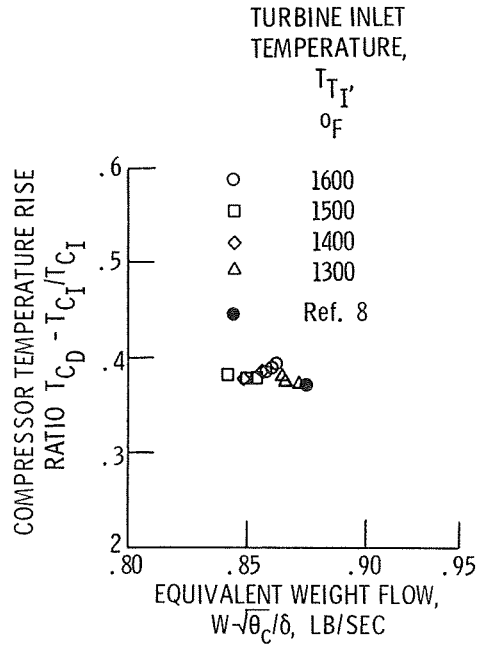

Figure 7. - Variation of compressor temperature rise ratio with equivalent flow rate.

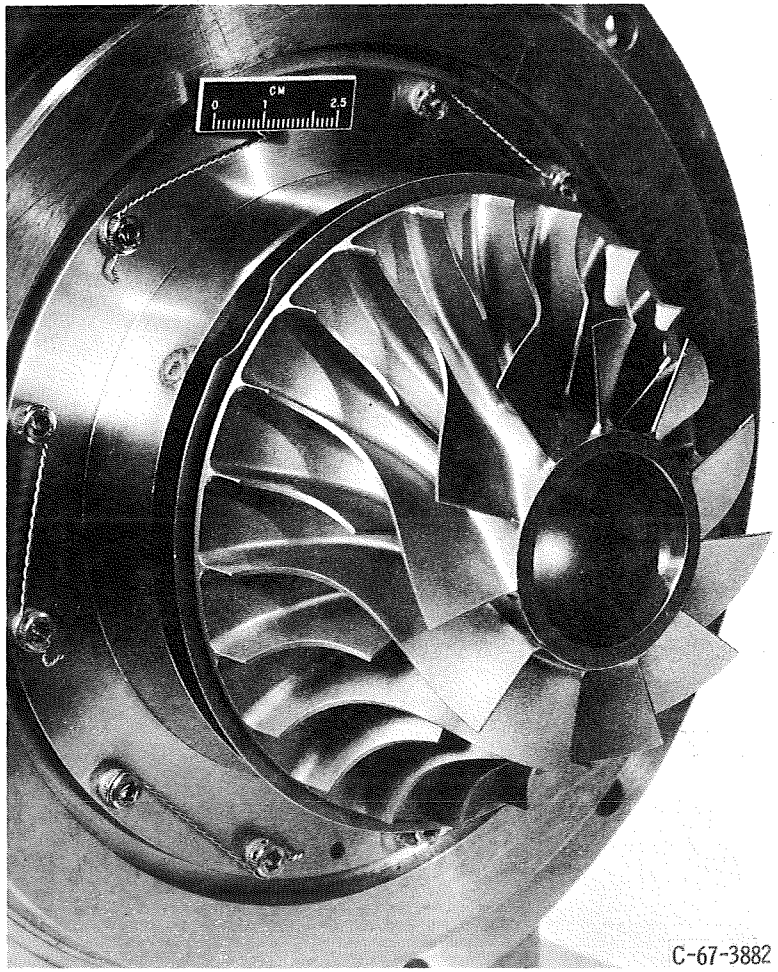

Figure 8. - Turbine rotor.

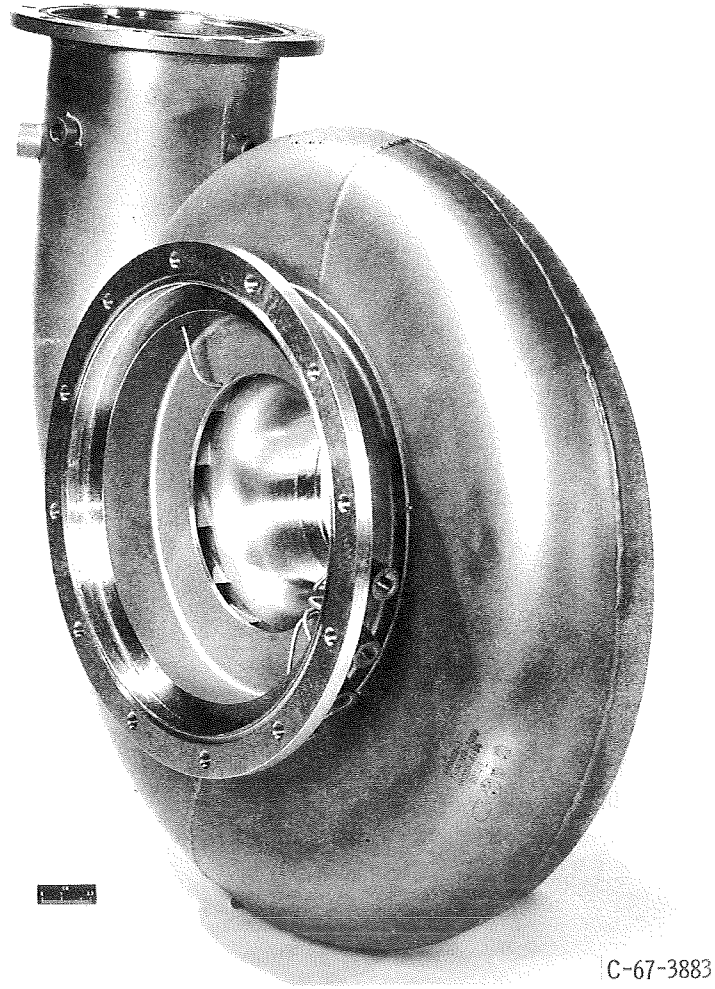

Figure 9. - Turbine scroll.

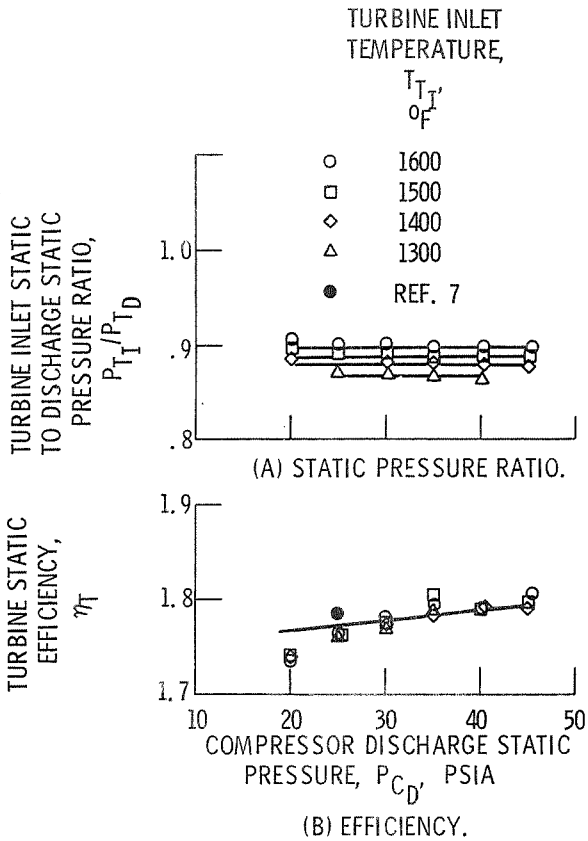

Figure 10. - Effect of compressor discharge pressure on turbine static pressure ratio and on efficiency.

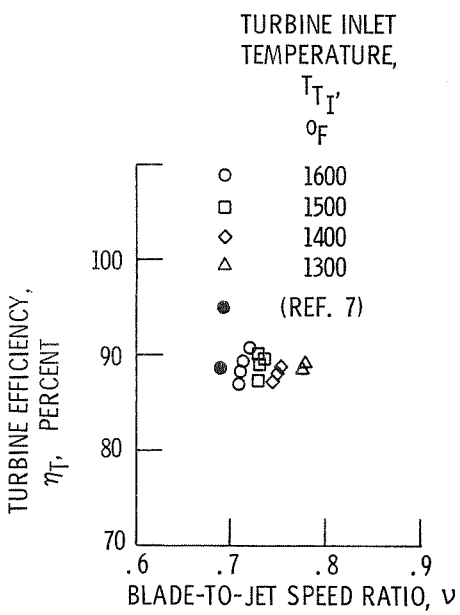

Figure 11. - Variation of turbine efficiency with blade-jet speed ratio.

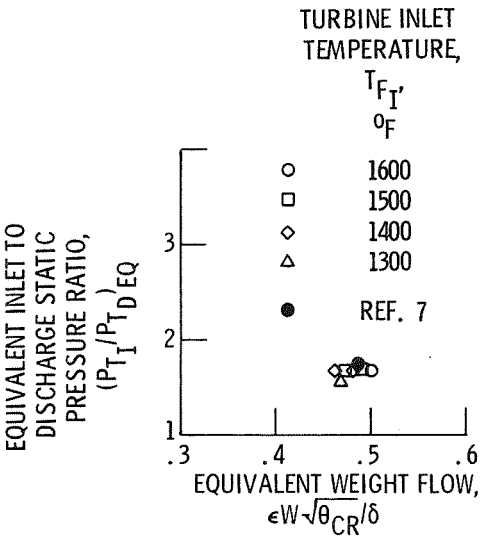

Figure 12. - Variation of turbine static pressure ratio with equivalent flow rate.

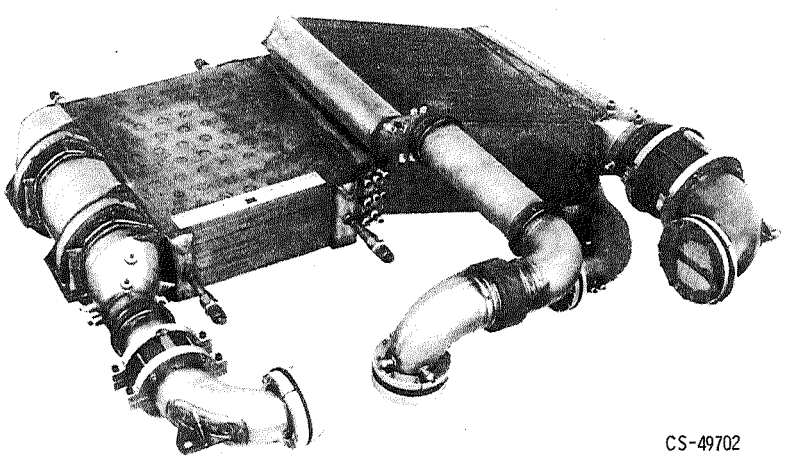

Figure 13. - Brayton heat exchanger unit.

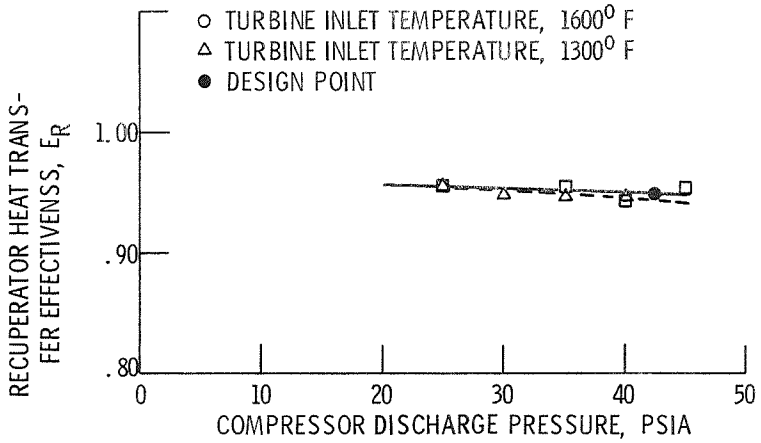

Figure 14. - Effects of turbine inlet temperature and pressure level on the recuperator effectiveness.

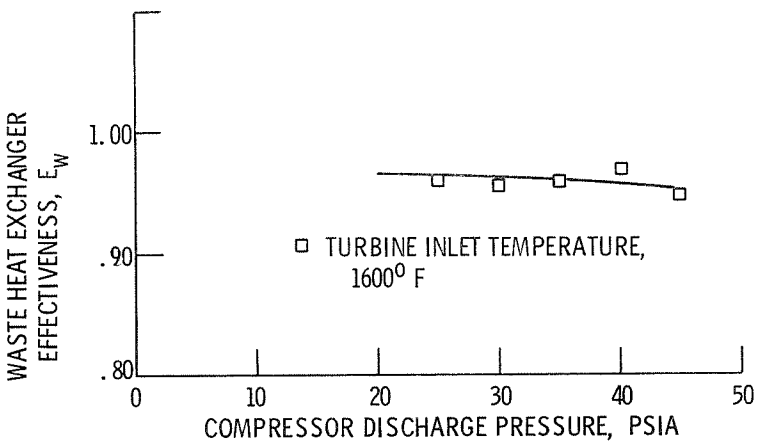

Figure 15. - Effect of pressure level on heat sink exchanger effectiveness.

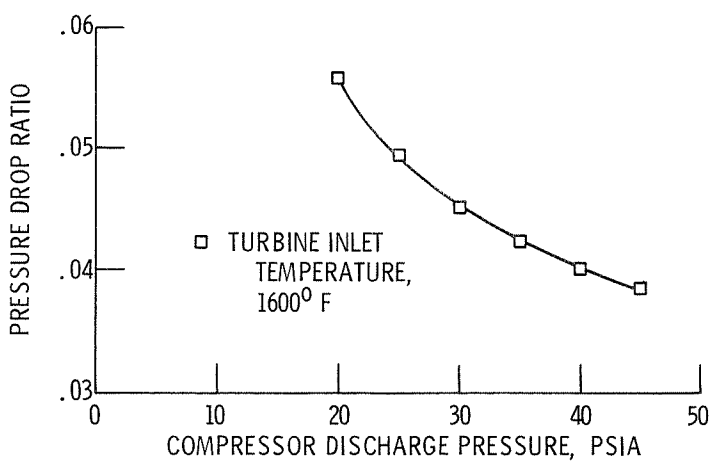

Figure 16. - Effect of pressure level on BHXU pressure drop.

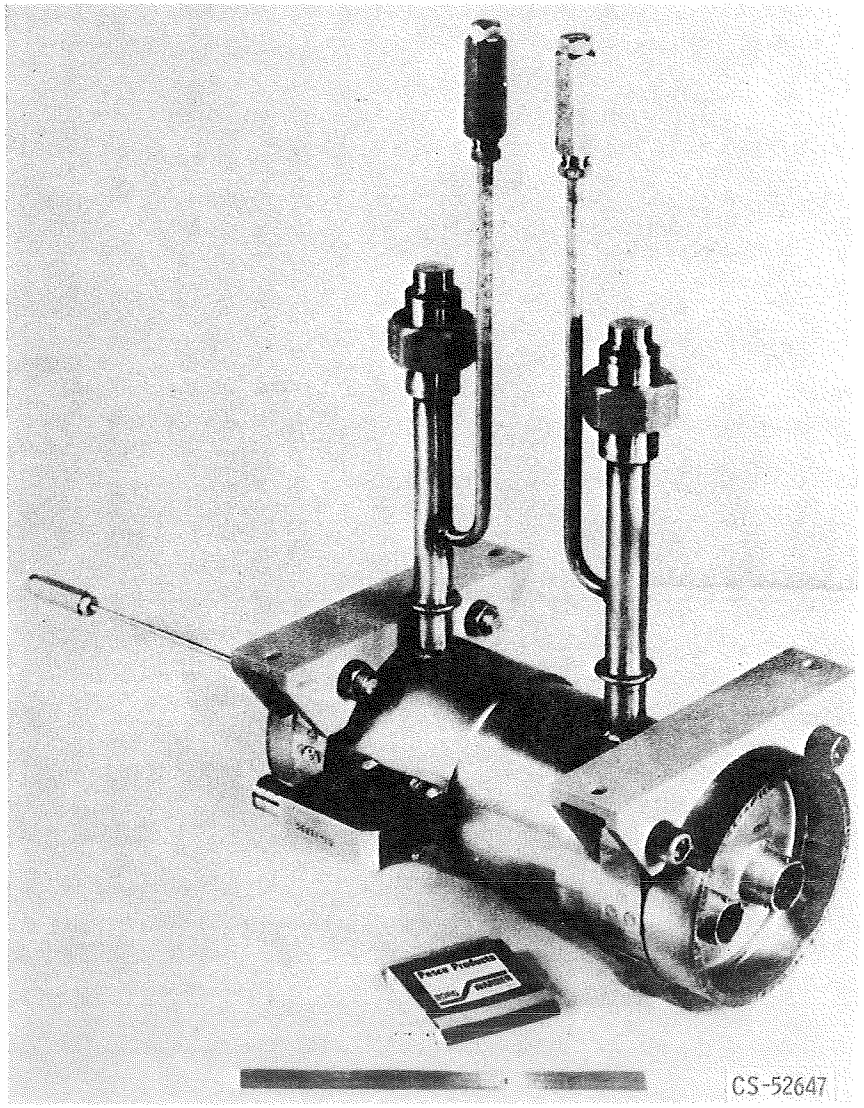

Figure 17. - Liquid coolant pump-motor assembly.

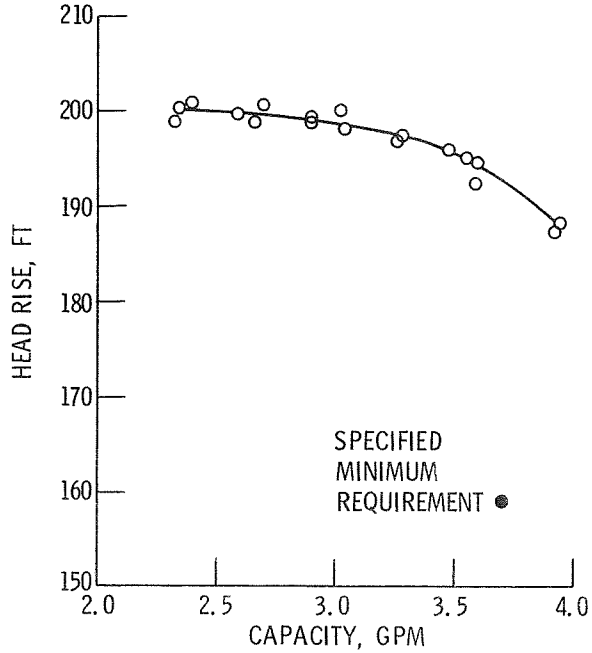

Figure 18. - Characteristic head curve of the liquid coolant pump.

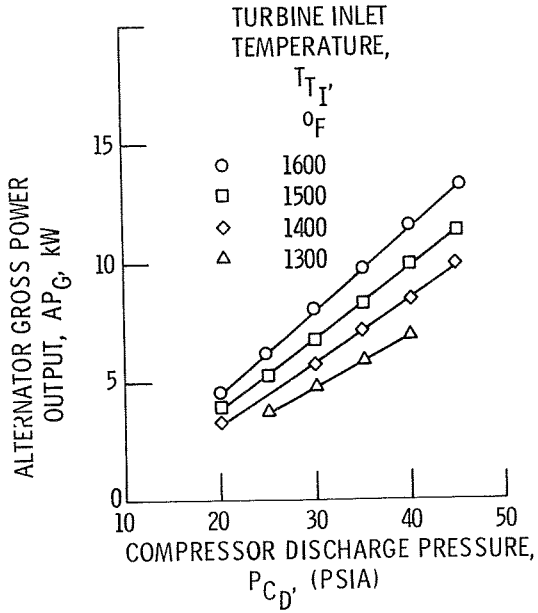

Figure 19. - Effect of system pressure level on the alternator gross power output.

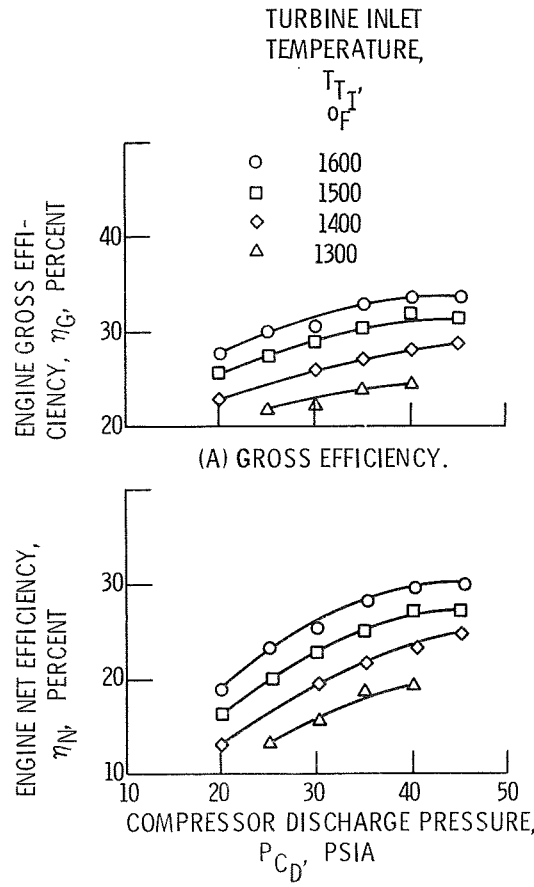

Figure 20. - Effect of system pressure level on the engine gross and net efficiencies.